

# Enhanced sensing of Stark weak field under the influence of Aubry-André-Harper criticality

Ayan Sahoo and Debraj Rakshit

Harish-Chandra Research Institute, A CI of Homi Bhabha National Institute, Chhatmag Road, Jhansi, Allahabad 211 019, India

The localization-delocalization transition can be leveraged as a resource for achieving quantum-enhanced sensitivity in parameter estimation. We demonstrate that by employing different classes of localization-delocalization transition potentials one can significantly enhance the precision of parameter estimation. Specifically, we focus on the precision measurement of the Stark strength parameter encoded in the ground state of a one-dimensional fermionic lattice under the influence of Aubry-André-Harper (AAH) localization-delocalization transition. We consider the single-particle system and the system at half-filling. Our work reveals that the Quantum Fisher Information (QFI) offers a superior scaling with respect to the system size in comparison to the pure Stark case, leading to a better parameter estimation. However, experimentally measuring fidelity-based QFI in a many-body system poses significant challenges. To address this, we suggest experimentally relevant operators that can be utilized to achieve precision surpassing the Heisenberg Limit (HL) or can even saturate the QFI scaling. These operators, relevant for practical experimental setups, provides a feasible pathway to harness the advantages offered by the localization-delocalization transition by exploiting two distinct localizing potentials for quantum-enhanced parameter estimation.

## I. INTRODUCTION

The ultimate limit of precision in parameter estimation is given by the Cramér-Rao bound [1–4]. For an unknown parameter,  $h$ , the standard deviation of parameter  $\delta h$  is bounded by a relation,  $\delta h \geq 1/\sqrt{MF_Q}$ , where  $M$  is the number of repetitions of the sensing protocol and  $F_Q$  is QFI. Classically, the QFI scales with  $L$  independent qubit as  $F_Q \sim L$ , known as a standard quantum limit (SQL), whereas it can reach Heisenberg limit (HL), i.e.,  $F_Q \sim L^2$ , for certain quantum mechanical systems [5–24]. There are some special kind of entangled states, such as the Greenberger-Horne-Zeilinger (GHZ) state that can be exploited for achieving HL. However, GHZ-based quantum sensors are susceptible to decoherence. Recently, various kinds of quantum many-body probes have been proposed for achieving quantum-enhanced sensitivity by harnessing the different types of quantum phenomena. In Quantum-many-Body (QMB) systems, like second order, localization-delocalization and topological phase transitions has been identified as a quantum resource for parameter sensing [7, 8, 25–29]. Other types of many-body probes that have been reported include quantum scars [30–33] and Floquet driving [12]. Generally, the precision of these probes can reach the HL. Moreover, sensing protocols with super-Heisenberg scaling have also been proposed recently on the QMB platform [7, 34–37]. In majority of the quantum critical sensors proposed so far, gap closing at criticality has been identified as the key ingredient driving quantum enhanced sensing. However, recently it has been demonstrated that symmetry-breaking at criticality can also be a crucial resource for quantum sensing [38].

QMB systems hosting distinct quantum phases can be used as a sensing probe. The unknown parameter to be estimated is encoded in the ground state or any excited state. These types of sensors may achieve HL at the criticality [39–41]. In order to estimate the parameter for these types of sensors we need to prepare a state and then adiabatically tune the parameter near criticality. This approach is referred as adiabatic sensing. In the critical region the system is extremely sensi-

tive to even a small change of the parameter. Consequently, the system has drastic response to the parameter change. As for an example, due to a self-dual symmetry, the AAH model shows localization-delocalization transition at a finite strength of the potential amplitude. This transition characterized by a quasi-periodic potential can be used as a resource for achieving quantum-enhanced parameter sensing that attains HL [42]. Recently, there has been proposals for quantum sensors using Stark localization. Interestingly, one can achieve super Heisenberg limit via Stark localization transition [43]. The QMB sensors have various applications in quantum technology [44–62]. At the critical point or transition point the fidelity susceptibility scales with system size  $L$  as  $L^{2/d\nu}$ , where  $d$  represents the spatial dimensionality of the system, and  $\nu$  is the critical exponent associated with the localization length,  $\zeta$ , near criticality ( $h_c$ ), such that  $\zeta \sim |h - h_c|^{-\nu}$ . At the transition point the precision of the unknown parameter  $h$  scales with system size as  $L^{2/\nu}$  [63, 64]. Experimentally, it is difficult to measure QFI. Therefore we need to find an experimentally measurable operator. For operators, one needs to compute operator based Fisher information (OFI) which is basically defined via signal-to-noise ratio. It can be shown that OFI is bounded by QFI [65]. In principle, the OFI saturates QFI when optimized over all possible operators.

The AAH model, characterized by tight-binding model with nearest-neighbor hopping and a quasiperiodic onsite potential, undergoes a localization-delocalization phase transition when the onsite potential's strength reaches twice the value of the hopping term [66]. The experimental evidence of this transition for AAH model has been reported in the ultracold atom setup [67–69] and in photonic crystals [70–73]. On the other hand, in the tight-binding model, if a linear gradient field is induced across the lattice instead of quasiperiodic potential, the system also shows localization-delocalization transition in the limit of zero-field strength. This is the case of well-known Stark localization [74–77]. In the context of the AAH model and the Stark model, the QFI exhibits distinct scaling behaviors at their respective criticalities. Specifically, at the criticality of the AAH model, the QFI scales with system size as  $L^2$  for single particle as well as half-filled probe,

which reaches the Heisenberg limit (HL). On the other hand, at the criticality of the Stark model, the QFI scales as  $L^{5.9}$  for single particle probe and  $L^{4.1}$  for half-filled probe, surpassing the Heisenberg limit [43]. Numerous studies have explored these critical phenomena individually in the presence of weak interactions [78, 79]. Recent studies have investigated the characteristic properties of fundamental physical quantities, such as localization length, inverse participation ratio, and energy gap, by examining systems in presence of these two different types of potentials. These studies reveal that the scaling exponents associated with the localization length, energy gap, and other related quantities are markedly different from the pure cases [80]. In this work, we investigate the advantage of interplay between these two potentials in the quantum sensing of stark weak field while initiating the system at the AAH criticality. Our results demonstrate that the precision of the parameter encoded in the Stark field potential can be significantly enhanced when measuring the parameter  $h$  in the presence of the AAH criticality. This suggests a novel approach to improve parameter estimation in quantum systems by leveraging the critical properties of different classes of quantum phase transitions, in general.

In the following, section I presents the introduction. Section II presents fidelity-based definition of QFI and OFI. The system is introduced in section III. Section IV demonstrates the behavior of QFI, OFIs, and their scaling with system size for a single-particle probe. Section V covers the QFI, OFIs, and their scaling for a many-body half-filled probe. Finally, the discussion is provided in section VI.

## II. PARAMETER ESTIMATION

If an unknown parameter  $h$  is encoded in a quantum state  $|\psi(h)\rangle$ , the fluctuation of the parameter near the  $h$  is captured by the fidelity susceptibility  $\chi_Q$  which is defined by

$$\chi_Q = - \lim_{\delta h \rightarrow 0} \frac{\partial^2 \mathcal{F}_Q}{\partial(\delta h)^2}, \quad (1)$$

where  $\mathcal{F}_Q = |\langle \psi(h) | \psi(h + \delta h) \rangle|$  is the distance between two nearby states  $|\psi(h)\rangle$  and  $|\psi(h + \delta h)\rangle$ . The QFI is related to fidelity susceptibility as  $\mathcal{F} = 4\chi_Q$  [8]. The estimation of an unknown parameter in experiment requires detecting average of an operator  $\hat{O}$ ,  $\langle \hat{O} \rangle = \text{Tr}[\hat{O}\rho(h)]$  in the function of  $h$ . where  $\rho(h)$  is the quantum state of the sensor. The sensitivity of  $h$  is quantified by the error propagation formula, which is essentially the signal-to-noise ratio, defined as

$$F_O = \lim_{\delta h \rightarrow 0} \frac{\left( \frac{d\langle \hat{O} \rangle}{d(\delta h)} \right)^2}{\text{Var}(\hat{O})}, \quad (2)$$

where  $\text{Var}(\hat{O})$  is defined as,  $\text{Var}(\hat{O}) = \langle \hat{O}^2 \rangle - \langle \hat{O} \rangle^2$ . The quantum Cramér-Rao bound [3, 4, 65] provides the bound on the uncertainty for any observable estimation:  $F_O(h, \hat{O}) \leq F_Q(h)$ .

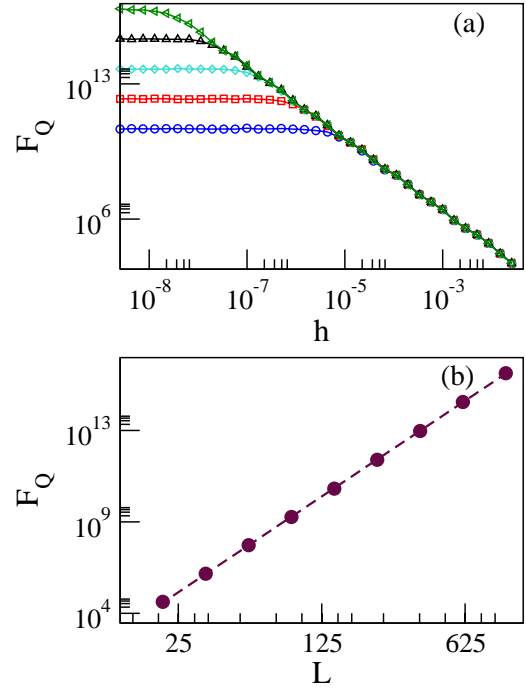


FIG. 1. **Single party QFI:** (a) presents QFI against the stark field  $h$  for system size  $L = 144$  (blue circle), 233 (red square), 377 (turquoise diamond), 610 (black triangular up), 987 (green triangular left). (b) shows the scaling plot. The maroon circles are QFI for different system sizes  $L = 21, 34, 55, 89, 144, 233, 377, 610$  at  $h = 10^{-9}$ , and the dotted line is the best fit  $F_Q \sim L^{6.7}$ . Both plots are shown in log-log scale. A configuration averaging over  $\phi$  is performed with 8000 random samples.

## III. SYSTEM

We consider a one-dimensional lattice with nearest-neighbor hopping in the presence of a quasi-periodically modulated potential and a linear gradient field, the so-called stark field. The generic form of Hamiltonian is  $\hat{H} = \hat{H}_0 + h\hat{H}_2$ . The explicit form of the Hamiltonian is given by,

$$\begin{aligned} \hat{H}_0 &= - \sum_i^{L-1} (\hat{c}_i^\dagger \hat{c}_{i+1} + \text{h.c.}) + V \sum_i^{L-1} \cos[2\pi(i\omega + \phi)] \hat{c}_i^\dagger \hat{c}_i, \\ \hat{H}_1 &= h \sum_i^{L-1} i \hat{c}_i^\dagger \hat{c}_i. \end{aligned} \quad (3)$$

where  $\hat{c}_i^\dagger$  ( $\hat{c}_i$ ) is creation (annihilation) operator and  $L$  denotes the system size. The first term in  $\hat{H}_0$  is the kinetic energy term. The lattice is subjected to two different kinds of onsite potentials. The second term in  $\hat{H}_0$  corresponds to a quasiperiodic onsite potential and  $H_1$  has contribution from the onsite potential energy due to the linear gradient field with strength  $h$ . Here  $\omega$  is taken as  $\omega = F_n/F_{n+1}$ , where  $F_n$  is the  $n^{\text{th}}$  Fibonacci number. For  $n \rightarrow \infty$  limit,  $\omega = \lim_{n \rightarrow \infty} F_n/F_{n+1} \rightarrow (\sqrt{5}-1)/2$ , which is golden ratio. In presence of the quasiperiodic potential, appropriate scaling

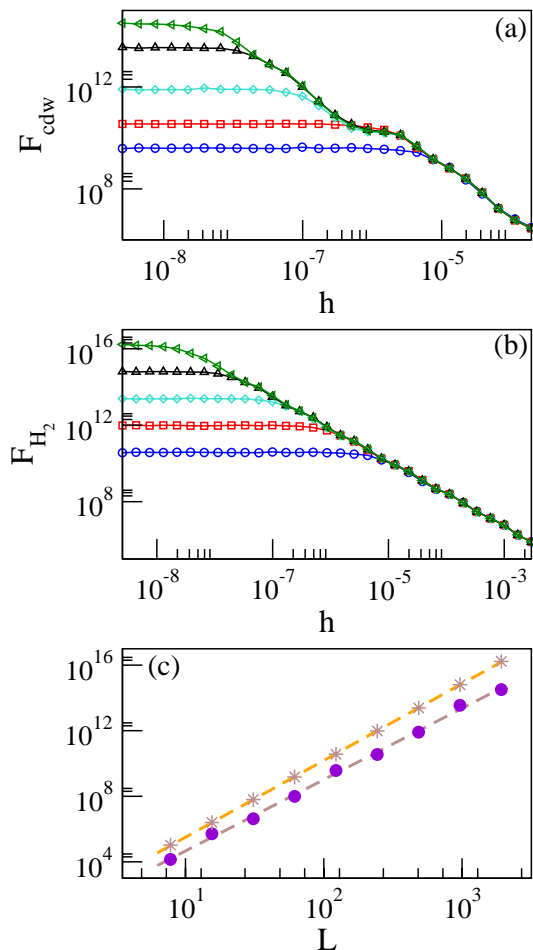


FIG. 2. **Single party OFI:** (a) presents OFI,  $F_{cdw}$ , for observable  $\hat{O}_{cdw}$  with respect to  $h$  for system size  $L = 144$  (blue circle), 233 (red square), 377 (turquoise diamond), 610 (black triangulat up), 987 (green triangular left). (b) presents OFI,  $F_{H_2}$  for observable  $\hat{O}_{H_2}$  with respect to  $h$  for system size  $L = 144$  (blue circle), 233 (red square), 377 (urquoise diamond), 610 (black triangulat up), 987 (green triangular left). (c) illustrates the scaling of OFI corresponding to the operator  $\hat{O}_{cdw}$ ,  $F_{cdw}$  (circles) and  $F_{H_2}$  (stars), respectively. The straight lines are the best fits. Whereas  $F_{cdw}$  scales as  $F_{cdw} \sim L^{6.2}$ ,  $F_{H_2}$  saturates the scaling of the QFI, i.e.,  $F_{H_2} \sim L^{6.7}$ .

emerges for the system sizes belonging to the fibonacci series [80].  $\phi$  is a phase which is chosen randomly from a uniform distribution in  $[0,1]$ . We consider open boundary condition (OBC). The Hamiltonian ( $\hat{H}$ ) reduces to pure stark case for  $V = 0$ . Then the system is localized in the zero field limit, i.e.,  $h \rightarrow 0$ . At this transition point the fidelity susceptibility scales with system size as  $\chi_Q \sim L^{2/\nu}$  with  $\nu = 0.33$  for single particle ground state [43]. Now, when the system is additionally at the criticality of AAH, i.e.,  $V = 2$ , the corresponding Hamiltonian is under the influence of two distinct onsite potentials. The scaling exponent associated with the localization-delocalization is reported as  $\nu = 0.29$  [80].

## IV. SINGLE PARTICLE SYSTEM AS PROBE

### A. Quantum Fisher Information

We first consider the single-particle scenario. Our goal is to perform precise measurement of  $h$  by setting the AAH potential at criticality. All eigen functions undergo delocalized to localized phase transition for this system. In the thermodynamic limit ( $L \rightarrow \infty$ ) the transition point takes place at  $h \rightarrow 0$  [43]. To address the question of whether the sensitivity of  $h$  can be enhanced using the criticality of the AAH model, we investigate and calculate both the QFI and the OFI in details.

In Fig. 1(a) we show QFI as a function of the stark strength  $h$  for  $V = 2$ , when the ground state of the system is exploited as a probe. We study various system sizes  $L = 144, 233, 377, 610, 987$ . Throughout the calculation, we have performed averaging over  $\phi$  for our single particle probe with OBC, where  $\phi$  is sampled randomly from a uniform distribution (see Eq. (3)). The figure illustrates that for a finite size system, as  $h$  enhances adiabatically, the QFI remains initially flat indicating an extended nature of the wavefunctions. The QFI starts decreasing beyond this flat region, which indicates entrance of the system into the localized phase. So, in the extended regions corresponding to the finite systems, there is a scaling of QFI with  $L$  whereas in the localized region, QFI becomes scale invariant, i.e., system size independent. Fig. 1(b) shows the scaling of QFI with finite system sizes in the extended region. The maroon circle is the value of QFI for different system sizes and the maroon dot-dot line is a fitting function  $F_Q \sim L^\beta$  with  $\beta = 6.7$ .

### B. Operator Fisher Information

Experimentally accessing the QFI poses significant challenges. So, we need to identify an observable that is both experimentally relevant and provides a significant quantum advantage in parameter estimation. We focus on the operator  $\hat{O}_{cdw} = \sum_i (-1)^i \hat{c}_i^\dagger \hat{c}_i$ , which measures the occupation imbalance between even and odd sites. This operator reveals the charge-density-wave (CDW) order in a quantum state and can be directly measured in optical lattice setups with ultracold atoms [67–69]. The computation of OFI is followed by the Eq. (2), which entails the average of  $\langle O_{cdw} \rangle$  and  $\langle \hat{O}_{cdw} \rangle^2$ , where,  $\langle \hat{O}_{cdw} \rangle^2 = \sum_{i,j} (-1)^{i+j} \hat{c}_i^\dagger \hat{c}_j^\dagger \hat{c}_j \hat{c}_i$ .

In Fig. 2(a), we plot OFI,  $F_{cdw}$ , versus  $h$ . In the finite-size system for the weak value of  $h$ , the  $F_{cdw}$  has a similar trend as QFI. Initially, it remains flat in the extended region, but after a certain value of  $h$ ,  $F_{cdw}$  gradually diminishes and it becomes system size invariant. From this figure,  $F_{cdw}$  increases with increasing system sizes in the extended region. The scaling of OFI with  $L$  is shown in Fig. 2(c). The violet circles represent the value of  $F_{cdw}$  in the extended region for various system sizes up to 987 and the brown dotted line is

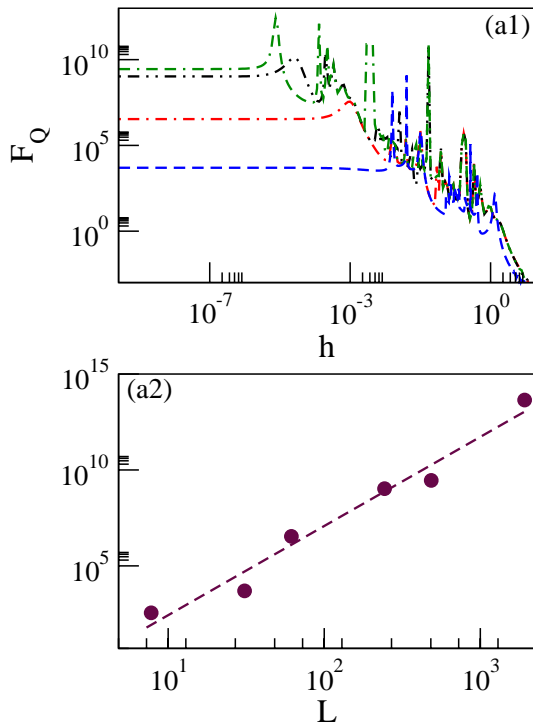


FIG. 3. **Half-filled case QFI:** (a1) QFI for half filled case with respect to  $h$ . We have taken system size  $L(n_f)$ , where  $L$  is system size and  $n_f$  is the number of filling. This figure shows that in the flat region, the QFI is increasing with system sizes,  $L = 55$  (28) (blue dash-dash), 89 (44) (red dot-dash), 233 (116) (black dot-dot-dash), 377 (188) (green dash-dash-dot). After a certain value of  $h$ , the QFI decays with certain initial fluctuations and again it shows steady behavior. (a2) In this plot we have shown the scaling of QFI with system size  $L(n_f)$ . The circle point is numerical value of QFI for  $h = 10^{-9}$  for  $L = 21$  (10), 55 (28), 89 (44), 233 (116), 377 (188), 987 (493) and the dotted line is the best fitting with fitting function  $F_Q(h = 10^{-9}) \sim L^{6.6}$ .

the fitting function  $F_{cdw} \sim L^\beta$  with  $\beta = 6.2$ . The scaling associated with  $F_{cdw}$  beats the Heisenberg limit (HL) and also the value of scaling exponent  $\beta$  is 6.2 which is higher than the scaling of QFI corresponding to the single-particle pure stark case. Hence, the experimentally realizable CDW observable offers a genuine quantum advantage in the measurement precision. We also consider another observable  $\hat{O}_{H_2} = \sum_i i \hat{c}_i^\dagger \hat{c}_i$ , which is essentially the last part of our Hamiltonian. In order to evaluate OFI for the operator  $\hat{O}_{H_2}$ , we need to evaluate the expectation values of the operator  $\langle \hat{O}_{H_2} \rangle$  and  $\langle \hat{O}_{H_2} \rangle^2$ , which is basically  $\langle \hat{O}_{H_2} \rangle^2 = \sum_{i,j} i j \hat{c}_i^\dagger \hat{c}_i \hat{c}_j^\dagger \hat{c}_j$ . In Fig. 2(b), we depict OFI,  $F_{H_2}$ , against  $h$  for various system sizes  $L$ . For a given system size  $L$ , the OFI, corresponding to the  $\hat{O}_{H_2}$  has a similar nature like  $F_{cdw}$ , i.e., initially for the small value of  $h$  the  $F_{H_2}$  is flat and after a certain value of  $h$ , it decreases gradually. There it becomes system size independent. However, the absolute value of OFI for  $\hat{O}_{H_2}$  is greater than  $F_{cdw}$ . In the flat region, the  $F_{H_2}$  increases steadily with system size  $L$ . The scaling of  $F_{H_2}$  in the extended region is shown in Fig. 2(c). The brown star illustrates the value of  $F_{H_2}$  at  $h = 10^{-9}$  with

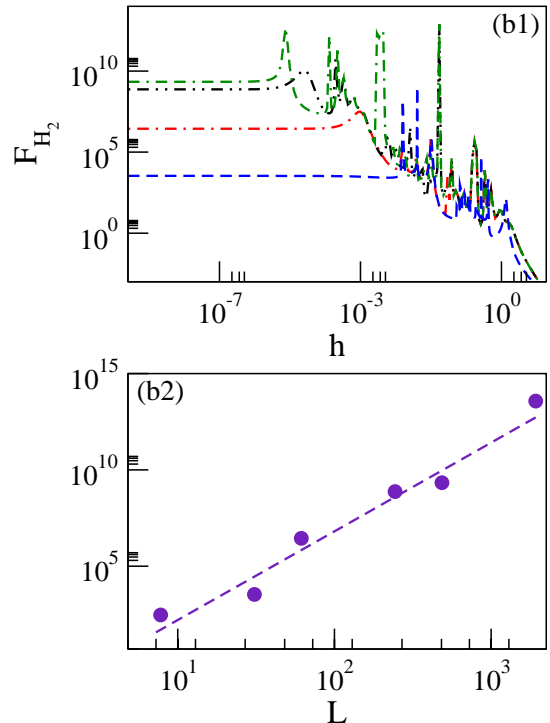


FIG. 4. **Half-filled case OFI:** (b1) The figure illustrates the behavior of the OFI for system size  $L(n_f)$  ( $n_f$  number of filling) with respect to  $h$ . In the flat region, the OFI increases with system size. However, after reaching a certain value of  $h$ , the OFI begins to decay with fluctuations and eventually stabilizes into a steady behavior. We have taken  $L = 55$  (blue dash-dash), 89 (red dot-dash), 233 (black dot-dot-dash), 377 (green dash-dash-dot). (b2) In this plot, we show the scaling of OFI with system size. The violet circular points represent the numerical values of OFI for  $h = 10^{-9}$  with  $L = 21$  (10), 55 (28), 89 (44), 233 (116), 377 (188), 987 (493), while the violet dotted line represents the best fit. We obtain  $F_{H_2}(h = 10^{-9}) \sim L^{6.6}$ .

different system sizes  $L$  up to 987, and the yellow dotted line is the fitting function of  $F_{H_2} \sim L^\beta$  with  $\beta = 6.7$ . This turns out to be a remarkable result as the scaling exponent for OFI  $\hat{O}_{H_2}$  saturates to that of the QFI.

## V. HALF-FILLED SYSTEM AS PROBE

We now focus on the half-filled case. We consider odd lattice sizes with OBC and the corresponding number of particles is either one of these two options:  $n_f = (L \pm 1)/2$ . We perform a slater determination method for this half-filled case. In order to construct the ground state configuration, we diagonalize the single-particle Hamiltonian and took the first  $n_f$  eigenvectors in a form of Slater determination. The ground state for half-filled case is given by,

$$\psi_0(j_1, \dots, j_{n_f}) = \frac{1}{\sqrt{n_f!}} \begin{vmatrix} \psi_1(j_1) & \dots & \psi_1(j_{n_f}) \\ \dots & \dots & \dots \\ \dots & \dots & \dots \\ \psi_{n_f}(j_1) & \dots & \psi_{n_f}(j_{n_f}) \end{vmatrix}, \quad (4)$$



where  $j$  runs from 1 to  $n_f$ . The fidelity for the half-filled ground state  $\psi_0$  is

$$f = |\langle \psi_0(h) | \psi_0(h + dh) \rangle|. \quad (5)$$

The general form of fidelity between  $\psi_0(h)$  and  $\psi_0(h + dh)$  is

$$f = |\langle \psi_0(h) | \psi_0(h + dh) \rangle| = \left| \begin{array}{ccc} P_{11} & \dots & P_{1n_f} \\ \dots & \dots & \dots \\ \dots & \dots & \dots \\ P_{n_f 1} & \dots & P_{n_f n_f} \end{array} \right|, \quad (6)$$

where  $P_{lm} = |\langle \psi_l(h) | \psi_m(h + dh) \rangle|$ .  $\psi_l, \psi_m$  are  $l$ 'th and  $m$ 'th eigenvectors. Now after Taylor series expansion, the fidelity can be written as

$$f = |\langle \psi_0(h) | \psi_0(h + dh) \rangle| = 1 - \frac{(\delta h)^2}{2} \chi, \quad (7)$$

where  $\chi = -\langle \psi_0 | \frac{d^2 \psi_0}{dh^2} \rangle$ . The fidelity susceptibility  $\chi = 2(1 - f)/dh^2$  and the corresponding QFI is  $F_Q = 4\chi$ .

We compute the ground state  $F_Q$  and  $F_{H_2}$  for system sizes up to 987 ( $n_f = 493$ ), where  $n_f$  is number of fermions. For the half-filled probe, we abstain from performing an averaging over  $\phi$ . We set  $\phi = 0$ . In the following, we describe the obtained results. Fig. 3(a1) illustrates the QFI for varying  $h$ . In a finite-size system, within the weak field region, where  $h$  is small, the QFI remains constant, exhibiting steady behavior. However, beyond a certain value of  $h$ , the QFI begins to fluctuate within a specific range due to the trade-off between AAH and the Stark strength. Eventually, its value decreases and stabilizes again. For the weak value of  $h$  in a finite-size system, the  $F_Q$  increases with system size in the flat region of  $F_Q$ . So, in this region, there is a scaling of  $F_Q$  with fitting function  $F_Q \sim L^\beta$ , where we find the scaling exponent  $\beta = 6.6$ . This is shown in Fig. 3(a2) with the maroon dotted line and the maroon circle is the numerical value of  $F_Q$  at  $h = 10^{-9}$ . The half-filled stark probe also achieves the super-Heisenberg limit with  $\beta = 6.6$ .

The operator  $\hat{O}_{cdw}$  is not ideal because the ground state lacks CDW ordering in the localized phase. This means that, unlike in the single-particle scenario, the OFI for  $\hat{O}_{cdw}$  does not exhibit proper scaling with  $L$ . However, the observable  $\hat{O}_{H_2} = \sum_i i \hat{c}_i^\dagger \hat{c}_i$  does provide an appropriate scaling. The corresponding OFI for the finite size system is shown in Fig. 4(b1). This figure illustrates the OFI as a function of  $h$ . Initially, for small values of  $h$ , the OFI remains relatively constant. However, beyond a certain threshold of  $h$ , the OFI starts to fluctuate. The fluctuations dissipate gradually and eventually stabilize again, similar to the behavior of the QFI. Additionally, the value of the OFI nearly converges to that of the QFI. In the flat region where OFI is not changing with  $h$ , the scaling of OFI for  $h = 10^{-9}$  is shown in Fig. 4(b2). The violet circle is the value of OFI at  $h = 10^{-9}$ , and the violet

dotted line is the fitting function of  $F_{H_2} \sim L^\beta$ , where  $\beta$  is 6.6. The scaling of OFI for observable  $\hat{O}_{H_2}$  is also saturated with the scaling of QFI. From Fig. 4(a1) and Fig. 4(b1), it is clear that the scaling sustains over an extended region, which is an added advantage over many quantum critical sensors for which quantum advantage is found over a very narrow region near the quantum criticality. For the half-filled system as a probe, the scaling of QFI beats the Heisenberg limit and gives the super Heisenberg scaling of 6.6. Also, for the half-filled probe, we got an observable that gives a super-Heisenberg scaling of  $\beta = 6.6$  saturating the scaling of QFI.

## VI. CONCLUSIONS

In the realm of quantum many-body systems, achieving super-Heisenberg limit precision remains a formidable challenge. This paper focuses on engineering efficient quantum many-body sensors. In an excellent recent new work it has been proposed that efficient weak field sensors can be designed by utilizing Stark localization as a resource [43]. Specifically, it has been demonstrated that under Stark localization, the quantum Fisher information (QFI) scales as  $L^6$ , i.e., a beyond-Heisenberg scaling is achieved.

This work proposes to use different classes of localization inducing potentials that can enhance the precision of parameter estimation even further. Our studies reveal that near the criticality of the AAH potential, better precision in estimating weak fields of Stark strength can be achieved with the QFI scaling as  $L^{6.7}$  in comparison to the pure Stark system for which the QFI is reported to scale as  $L^6$ . In addition, this work proposes an experimentally accessible observable, the charge-density-wave (CDW) order denoted as  $\hat{O}_{cdw}$ . Remarkably, this observable also exhibits super-Heisenberg scaling with the QFI scaling as  $F_{cdw} \sim L^{6.2}$ . Moreover, another observable,  $\hat{O}_{H_2}$ , has been identified for which the associated OFI not only saturates to the QFI but also matches the scaling behavior of the QFI. For many-body systems, particularly under the condition of half-filling, the scaling of the QFI with system size is found as  $F_Q \sim L^{6.6}$ . Similarly, for the half-filled case, the OFI corresponding to the operator  $\hat{O}_{H_2}$  exhibits the same scaling behavior as the QFI, that is  $F_{H_2} \sim L^{6.6}$ .

In summary, our work proposes an experimentally realizable protocol for achieving enhanced sensing of the Stark weak field by invoking another type of localization-inducing potential in form of the AAH potential and by exploiting the AAH criticality. One may, in principle, envision the underlying strength of the concept which can, in principle, be generalized for criticality based quantum sensors – In context of precision estimation of an unknown parameter within the QMB platform, it might be advantageous to introduce additional control parameters, that, in turn, introduces new kinds of quantum criticality, for obtaining enhanced quantum advantage by utilizing the competing effects of multiple critical points.

- [1] S. L. Braunstein and C. M. Caves, Statistical distance and the geometry of quantum states, *Phys. Rev. Lett.* **72**, 3439 (1994).
- [2] C. L. Degen, F. Reinhard, and P. Cappellaro, Quantum sensing, *Rev. Mod. Phys.* **89**, 035002 (2017).
- [3] H. Cramér, *Mathematical Methods of Statistics (PMS-9), Volume 9* (Princeton University Press, Princeton, 1946).
- [4] C. W. Helstrom, Quantum detection and estimation theory, *Journal of Statistical Physics* **1**, 231 (1969).
- [5] V. Giovannetti, S. Lloyd, and L. Maccone, Quantum-enhanced measurements: beating the standard quantum limit, *Science* **306**, 1330 (2004).
- [6] V. Giovannetti, S. Lloyd, and L. Maccone, Quantum metrology, *Phys. Rev. Lett.* **96**, 010401 (2006).
- [7] M. M. Rams, P. Sierant, O. Dutta, P. Horodecki, and J. Zakrzewski, At the limits of criticality-based quantum metrology: Apparent super-heisenberg scaling revisited, *Phys. Rev. X* **8**, 021022 (2018).
- [8] P. Zanardi, M. G. A. Paris, and L. Campos Venuti, Quantum criticality as a resource for quantum estimation, *Phys. Rev. A* **78**, 042105 (2008).
- [9] L. Campos Venuti and P. Zanardi, Quantum critical scaling of the geometric tensors, *Phys. Rev. Lett.* **99**, 095701 (2007).
- [10] M. Tsang, Quantum transition-edge detectors, *Phys. Rev. A* **88**, 021801 (2013).
- [11] L. Garbe, M. Bina, A. Keller, M. G. A. Paris, and S. Felicetti, Critical quantum metrology with a finite-component quantum phase transition, *Phys. Rev. Lett.* **124**, 120504 (2020).
- [12] U. Mishra and A. Bayat, Driving enhanced quantum sensing in partially accessible many-body systems, *Phys. Rev. Lett.* **127**, 080504 (2021).
- [13] K. Gietka, F. Metz, T. Keller, and J. Li, Adiabatic critical quantum metrology cannot reach the Heisenberg limit even when shortcuts to adiabaticity are applied, *Quantum* **5**, 489 (2021).
- [14] Y. Chu, S. Zhang, B. Yu, and J. Cai, Dynamic framework for criticality-enhanced quantum sensing, *Phys. Rev. Lett.* **126**, 010502 (2021).
- [15] M. Salado-Mejía, R. Román-Ancheyta, F. Soto-Eguibar, and H. M. Moya-Cessa, Spectroscopy and critical quantum thermometry in the ultrastrong coupling regime, *Quantum Science and Technology* **6**, 025010 (2021).
- [16] V. Montenegro, U. Mishra, and A. Bayat, Global sensing and its impact for quantum many-body probes with criticality, *Phys. Rev. Lett.* **126**, 200501 (2021).
- [17] S. S. Mirkhalaf, E. Witkowska, and L. Lepori, Supersensitive quantum sensor based on criticality in an antiferromagnetic spinor condensate, *Phys. Rev. A* **101**, 043609 (2020).
- [18] I. Frérot and T. Roscilde, Quantum critical metrology, *Phys. Rev. Lett.* **121**, 020402 (2018).
- [19] P. Zanardi and N. Paunković, Ground state overlap and quantum phase transitions, *Phys. Rev. E* **74**, 031123 (2006).
- [20] W.-L. You, Y.-W. Li, and S.-J. Gu, Fidelity, dynamic structure factor, and susceptibility in critical phenomena, *Phys. Rev. E* **76**, 022101 (2007).
- [21] P. Zanardi, P. Giorda, and M. Cozzini, Information-theoretic differential geometry of quantum phase transitions, *Phys. Rev. Lett.* **99**, 100603 (2007).
- [22] D. Braun, G. Adesso, F. Benatti, R. Floreanini, U. Marzolino, M. W. Mitchell, and S. Pirandola, Quantum-enhanced measurements without entanglement, *Rev. Mod. Phys.* **90**, 035006 (2018).
- [23] T. Ilias, D. Yang, S. F. Huelga, and M. B. Plenio, Criticality-enhanced quantum sensing via continuous measurement, *PRX Quantum* **3**, 010354 (2022).
- [24] D. Yang, S. F. Huelga, and M. B. Plenio, Efficient information retrieval for sensing via continuous measurement, *Phys. Rev. X* **13**, 031012 (2023).
- [25] W. DeGottardi, D. Sen, and S. Vishveshwara, Majorana fermions in superconducting 1d systems having periodic, quasiperiodic, and disordered potentials, *Phys. Rev. Lett.* **110**, 146404 (2013).
- [26] X. Cai, L.-J. Lang, S. Chen, and Y. Wang, Topological superconductor to anderson localization transition in one-dimensional incommensurate lattices, *Phys. Rev. Lett.* **110**, 176403 (2013).
- [27] J. Fraxanet, U. Bhattacharya, T. Grass, D. Rakshit, M. Lewenstein, and A. Dauphin, Topological properties of the long-range kitaev chain with aubry-andré-harper modulation, *Phys. Rev. Res.* **3**, 013148 (2021).
- [28] K. Macieszczak, M. u. u. u. Guță, I. Lesanovsky, and J. P. Garrahan, Dynamical phase transitions as a resource for quantum enhanced metrology, *Phys. Rev. A* **93**, 022103 (2016).
- [29] L. Garbe, O. Abah, S. Felicetti, and R. Puebla, Critical quantum metrology with fully-connected models: from heisenberg to kibble-zurek scaling, *Quantum Science and Technology* **7**, 035010 (2022).
- [30] S. Dooley, S. Pappalardi, and J. Goold, Entanglement enhanced metrology with quantum many-body scars, *Phys. Rev. B* **107**, 035123 (2023).
- [31] A. Yoshinaga, Y. Matsuzaki, and R. Hamazaki, Quantum metrology protected by hilbert space fragmentation, arXiv preprint arXiv:2211.09567 (2022).
- [32] J.-Y. Desaulles, A. Hudomal, C. J. Turner, and Z. Papić, Proposal for realizing quantum scars in the tilted 1d fermi-hubbard model, *Phys. Rev. Lett.* **126**, 210601 (2021).
- [33] S. Dooley, Robust quantum sensing in strongly interacting systems with many-body scars, *PRX Quantum* **2**, 020330 (2021).
- [34] S.-J. Gu, H.-M. Kwok, W.-Q. Ning, and H.-Q. Lin, Fidelity susceptibility, scaling, and universality in quantum critical phenomena, *Phys. Rev. B* **77**, 245109 (2008).
- [35] B.-B. Wei, Fidelity susceptibility in one-dimensional disordered lattice models, *Phys. Rev. A* **99**, 042117 (2019).
- [36] S. Boixo, S. T. Flammia, C. M. Caves, and J. Geremia, Generalized limits for single-parameter quantum estimation, *Phys. Rev. Lett.* **98**, 090401 (2007).
- [37] S. M. Roy and S. L. Braunstein, Exponentially enhanced quantum metrology, *Phys. Rev. Lett.* **100**, 220501 (2008).
- [38] S. Mondal, A. Sahoo, U. Sen, and D. Rakshit, *Multicritical quantum sensors driven by symmetry-breaking* (2024), arXiv:2407.14428 [quant-ph].
- [39] S.-J. Gu and W. C. Yu, Spectral function and fidelity susceptibility in quantum critical phenomena, *Europhysics Letters* **108**, 20002 (2014).
- [40] J. Zhang, X. Peng, N. Rajendran, and D. Suter, Detection of quantum critical points by a probe qubit, *Phys. Rev. Lett.* **100**, 100501 (2008).
- [41] J. Zhang, F. M. Cucchietti, C. M. Chandrashekar, M. Laforest, C. A. Ryan, M. Ditty, A. Hubbard, J. K. Gamble, and R. Laflamme, Direct observation of quantum criticality in ising spin chains, *Phys. Rev. A* **79**, 012305 (2009).
- [42] A. Sahoo, U. Mishra, and D. Rakshit, Localization-driven quantum sensing, *Phys. Rev. A* **109**, L030601 (2024).
- [43] X. He, R. Yousefjani, and A. Bayat, Stark localization as a re-

- source for weak-field sensing with super-heisenberg precision, *Phys. Rev. Lett.* **131**, 010801 (2023).
- [44] D. O. J. Appel, P. J. Windpassinger and E. S. Polzik, Mesoscopic atomic entanglement for precision measurements beyond the standard quantum limit, *Proc. Natl. Acad. Sci. USA* **106**, 10960 (2009).
- [45] A. Louchet-Chauvet, J. Appel, J. J. Renema, D. Oblak, N. Kjaergaard, and E. S. Polzik, Entanglement-assisted atomic clock beyond the projection noise limit, *New Journal of Physics* **12**, 065032 (2010).
- [46] L. Pezzè, A. Smerzi, M. K. Oberthaler, R. Schmied, and P. Treutlein, Quantum metrology with nonclassical states of atomic ensembles, *Rev. Mod. Phys.* **90**, 035005 (2018).
- [47] S. F. Huelga, C. Macchiavello, T. Pellizzari, A. K. Ekert, M. B. Plenio, and J. I. Cirac, Improvement of frequency standards with quantum entanglement, *Phys. Rev. Lett.* **79**, 3865 (1997).
- [48] M. Ozmaniec, R. Augusiak, C. Gogolin, J. Kołodyński, A. Acín, and M. Lewenstein, Random bosonic states for robust quantum metrology, *Phys. Rev. X* **6**, 041044 (2016).
- [49] H. Zhou, J. Choi, S. Choi, R. Landig, A. M. Douglas, J. Isoya, F. Jelezko, S. Onoda, H. Sumiya, P. Cappellaro, H. S. Knowles, H. Park, and M. D. Lukin, Quantum metrology with strongly interacting spin systems, *Phys. Rev. X* **10**, 031003 (2020).
- [50] J. Naikoo, R. W. Chhajlany, and J. Kołodyński, Multiparameter estimation perspective on non-hermitian singularity-enhanced sensing, *Phys. Rev. Lett.* **131**, 220801 (2023).
- [51] G. D. Fresco, B. Spagnolo, D. Valenti, and A. Carollo, Multiparameter quantum critical metrology, *SciPost Phys.* **13**, 077 (2022).
- [52] G. Mihailescu, A. Bayat, S. Campbell, and A. K. Mitchell, Multiparameter critical quantum metrology with impurity probes, *Quantum Science and Technology* **9**, 035033 (2024).
- [53] R. Yousefjani, X. He, A. Carollo, and A. Bayat, Nonlinearity-enhanced quantum sensing in stark probes, arXiv preprint arXiv:2404.10382 (2024).
- [54] V. Mourik, K. Zuo, S. M. Frolov, S. Plissard, E. P. Bakkers, and L. P. Kouwenhoven, Signatures of majorana fermions in hybrid superconductor-semiconductor nanowire devices, *Science* **336**, 1003 (2012).
- [55] M. T. Deng, C. L. Yu, G. Y. Huang, M. Larsson, P. Caroff, and H. Q. Xu, Anomalous zero-bias conductance peak in a nb-insb nanowire-nb hybrid device, *Nano Letters* **12**, 6414 (2012).
- [56] A. Das, Y. Ronen, Y. Most, Y. Oreg, M. Heiblum, and H. Shtrikman, Zero-bias peaks and splitting in an al-inas nanowire topological superconductor as a signature of majorana fermions, *Nature Physics* **8**, 887 (2012).
- [57] I. C. Fulga, A. Haim, A. R. Akhmerov, and Y. Oreg, Adaptive tuning of majorana fermions in a quantum dot chain, *New Journal of Physics* **15**, 045020 (2013).
- [58] S. Nadj-Perge, I. K. Drozdov, J. Li, H. Chen, S. Jeon, J. Seo, A. H. MacDonald, B. A. Bernevig, and A. Yazdani, Observation of majorana fermions in ferromagnetic atomic chains on a superconductor, *Science* **346**, 602 (2014), <https://www.science.org/doi/pdf/10.1126/science.1259327>.
- [59] J.-S. Xu, K. Sun, Y.-J. Han, C.-F. Li, J. K. Pachos, and G.-C. Guo, Simulating the exchange of majorana zero modes with a photonic system, *Nature Communications* **7**, 13194 (2016).
- [60] Y. Xing, L. Qi, J. Cao, D.-Y. Wang, C.-H. Bai, W.-X. Cui, H.-F. Wang, A.-D. Zhu, and S. Zhang, Controllable photonic and phononic edge localization via optomechanically induced kitaev phase, *Opt. Express* **26**, 16250 (2018).
- [61] T. Dvir, G. Wang, N. van Loo, C.-X. Liu, G. P. Mazur, A. Bordin, S. L. D. ten Haaf, J.-Y. Wang, D. van Driel, F. Zatelli, X. Li, F. K. Malinowski, S. Gazibegovic, G. Badawy, E. P. A. M. Bakkers, M. Wimmer, and L. P. Kouwenhoven, Realization of a minimal kitaev chain in coupled quantum dots, *Nature* **614**, 445 (2023).
- [62] H. Manshouri, M. Zarei, M. Abdi, S. Bose, and A. Bayat, Quantum enhanced sensitivity through many-body bloch oscillations, arXiv preprint arXiv:2406.13921 (2024).
- [63] M. Thakurathi, D. Sen, and A. Dutta, Fidelity susceptibility of one-dimensional models with twisted boundary conditions, *Phys. Rev. B* **86**, 245424 (2012).
- [64] T. Cookmeyer, J. Motruk, and J. E. Moore, Critical properties of the ground-state localization-delocalization transition in the many-particle aubry-andré model, *Phys. Rev. B* **101**, 174203 (2020).
- [65] L. Pezzè, A. Trenkwalder, and M. Fattori, Adiabatic sensing enhanced by quantum criticality, arXiv preprint arXiv:1906.01447 (2019).
- [66] S. Aubry and G. André, Anderson localization for onedimensional difference schrödinger operator with quasiperiodic potential, *Ann. Isr. Phys. Soc.* **3** (1980).
- [67] M. Schreiber, S. S. Hodgman, P. Bordia, H. P. Lüschen, M. H. Fischer, R. Vosk, E. Altman, U. Schneider, and I. Bloch, Observation of many-body localization of interacting fermions in a quasirandom optical lattice, *Science* **349**, 842 (2015), <https://www.science.org/doi/pdf/10.1126/science.aaa7432>.
- [68] L. Dal Negro, C. J. Oton, Z. Gaburro, L. Pavesi, P. Johnson, A. Lagendijk, R. Righini, M. Colocci, and D. S. Wiersma, Light transport through the band-edge states of fibonacci quasicrystals, *Phys. Rev. Lett.* **90**, 055501 (2003).
- [69] G. Modugno, Anderson localization in bose-einstein condensates, *Reports on Progress in Physics* **73**, 102401 (2010).
- [70] Y. Lahini, R. Pugatch, F. Pozzi, M. Sorel, R. Morandotti, N. Davidson, and Y. Silberberg, Observation of a localization transition in quasiperiodic photonic lattices, *Phys. Rev. Lett.* **103**, 013901 (2009).
- [71] Y. E. Kraus, Y. Lahini, Z. Ringel, M. Verbin, and O. Zeitlinger, Topological states and adiabatic pumping in quasicrystals, *Phys. Rev. Lett.* **109**, 106402 (2012).
- [72] M. Verbin, O. Zeitlinger, Y. E. Kraus, Y. Lahini, and Y. Silberberg, Observation of topological phase transitions in photonic quasicrystals, *Phys. Rev. Lett.* **110**, 076403 (2013).
- [73] M. Verbin, O. Zeitlinger, Y. Lahini, Y. E. Kraus, and Y. Silberberg, Topological pumping over a photonic fibonacci quasicrystal, *Phys. Rev. B* **91**, 064201 (2015).
- [74] G. H. Wannier, Wave functions and effective hamiltonian for bloch electrons in an electric field, *Phys. Rev.* **117**, 432 (1960).
- [75] H. Fukuyama, R. A. Bari, and H. C. Fogedby, Tightly bound electrons in a uniform electric field, *Phys. Rev. B* **8**, 5579 (1973).
- [76] X.-P. Jiang, R. Qi, S. Yang, Y. Hu, and G. Yang, Stark many-body localization with long-range interactions, arXiv preprint arXiv:2307.12376 (2023).
- [77] X. Wei, X. Gao, and W. Zhu, Static and dynamical stark many-body localization transition in a linear potential, *Phys. Rev. B* **106**, 134207 (2022).
- [78] V. P. Michal, B. L. Altshuler, and G. V. Shlyapnikov, Delocalization of weakly interacting bosons in a 1d quasiperiodic potential, *Phys. Rev. Lett.* **113**, 045304 (2014).
- [79] S. Iyer, V. Oganessian, G. Refael, and D. A. Huse, Many-body localization in a quasiperiodic system, *Phys. Rev. B* **87**, 134202 (2013).
- [80] A. Sahoo, A. Saha, and D. Rakshit, Stark localization near aubry-andré criticality, arXiv preprint arXiv:2404.14971 (2024).